Role of Direct Laser Acceleration of Electrons in a Laser Wakefield Accelerator with Ionization Injection

J. L. Shaw,[1,*] N. Lemos,[1,†] L. D. Amorim,[2,3] N. Vafaei-Najafabadi,[1,‡] K. A. Marsh,[1] F. S. Tsung,[2]
W. B. Mori,[1,2] and C. Joshi[1]

[1]*University of California Los Angeles Department of Electrical Engineering, Los Angeles, California 90095, USA*
[2]*University of California Los Angeles Department of Physics and Astronomy, Los Angeles, California 90095, USA*
[3]*GoLP/Instituto de Plasmas e Fusão Nuclear, Instituto Superior Técnico, Universidade de Lisboa, 1049-001 Lisbon, Portugal*

We show the first experimental demonstration that electrons being accelerated in a laser wakefield accelerator operating in the forced or blowout regimes gain significant energy from both the direct laser acceleration (DLA) and the laser wakefield acceleration mechanisms. Supporting full-scale 3D particle-in-cell simulations elucidate the role of the DLA of electrons in a laser wakefield accelerator when ionization injection of electrons is employed. An explanation is given for how electrons can maintain the DLA resonance condition in a laser wakefield accelerator despite the evolving properties of both the drive laser and the electrons. The produced electron beams exhibit characteristic features that are indicative of DLA as an additional acceleration mechanism.

The transverse, oscillating electric fields at the focus of PW-class lasers can reach TeV/cm and yet cannot synchronously accelerate charged particles to very high energies in vacuum [1]. One way around this limitation is to focus such intense but short laser pulses in plasmas to excite charge density waves (wakes) that propagate at nearly the speed of light [2]. These wakes have substantial accelerating longitudinal fields (100s GeV/m), which can transfer the energy of the laser pulse to charged particles. This method is known as a laser wakefield accelerator (LWFA) [3]. In this Letter, we show that in addition to wakefield acceleration, LWFAs can have all the conditions needed to transfer energy from the laser field to the electrons via a process known as direct laser acceleration (DLA) [4–10]. This process can be exploited to microbunch electron beams on attosecond time scales [11] or to enhance the x-ray radiation produced by betatron motion of electrons in LWFA [12,13].

In our experiment, we use ionization injection [14,15] to place charge into the plasma accelerator structure such that it overlaps with the laser pulse. Under such conditions, the contribution of DLA to the energy of the accelerated electrons can be comparable to that of the wakefield. While the contribution of DLA to the electron energy gain had been anticipated in previous work [16–22], there was no direct experimental evidence for DLA in the accelerated electron spectra in these studies. In this Letter, we experimentally demonstrate that the energy gain of the electrons due to DLA in a nonlinear LWFA can be discerned through characteristic spectral features that are reproduced in particle-in-cell (PIC) simulations.

In the matched blowout regime of LWFA [23], the radiation pressure of an intense laser pulse can push a majority of the plasma electrons out and around the body of the pulse. The expelled plasma electrons feel the electrostatic field of the relatively stationary ions and are attracted back towards the laser axis behind the laser pulse. They overshoot the axis and set up a wake oscillation, which can trap electrons at the rear of the wake where those electrons are accelerated by the longitudinal wakefield as shown in Fig. 1(a). Those electrons injected off axis undergo betatron oscillations in response to the linear transverse focusing force of the ions [24,25].

In contrast to the matched case shown in Fig. 1(a), where the laser pulse is only filling the front portion of the first period (bucket) of the wake, Fig. 1(b) illustrates a LWFA also operating in a near-complete blowout regime but where the laser pulse is long enough to overlap the ionization-injected electrons trapped in the first bucket. In this configuration, the betatron oscillations of the electrons in the plane of the laser polarization can lead to an energy transfer from the transverse electric field of the laser to the transverse momentum of the electrons. This enhanced transverse momentum can then be converted into increased longitudinal momentum via the $\mathbf{v} \times \mathbf{B}$ force of the laser. This process is known as DLA [4,5]. Unlike the trapped electrons with small betatron oscillation amplitudes seen in Fig. 1(a), in Fig. 1(b) the trapped charge becomes modulated at the half-laser wavelength [11] and has a transverse extent that is on the order of the local radius of the wake.

The energy gained by the electrons due to the transverse electric field $\mathbf{E}_\perp$ is calculated from the integral

$$W_\perp = -e \int_0^t \mathbf{E}_\perp \cdot \mathbf{v}_\perp \, dt', \tag{1}$$

where $\mathbf{v}_\perp$ is the transverse velocity of the electron. The dominant transverse electric field is the laser electric field,
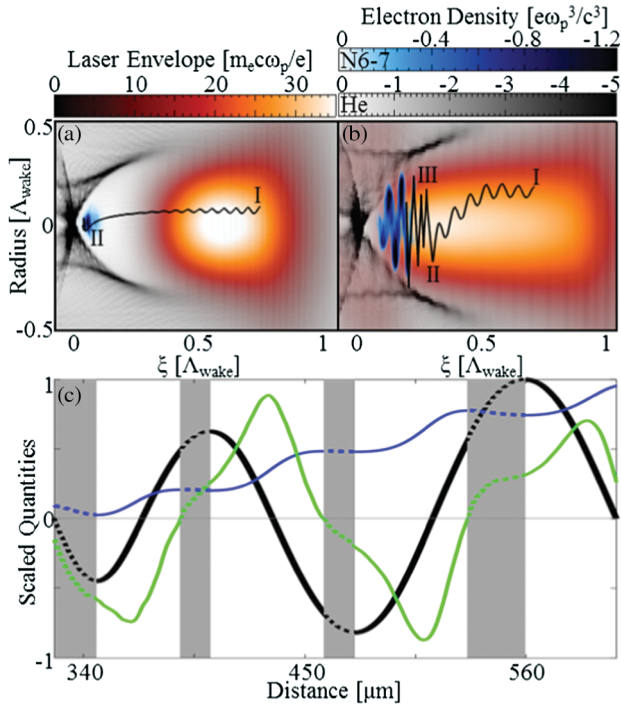
FIG. 1.   Instantaneous OSIRIS simulation snapshots of a LWFA operating in the (a) short-pulse blowout regime and the (b) quasi-blowout regime where the drive laser overlaps the trapped electrons. The black curve is the trajectory of an electron in the wake frame over the entire duration of its acceleration (i.e., many time steps, not an instantaneous snapshot). This electron is born via ionization injection at "I" and slips back relative to the wakefield until it is trapped at "II" and begins executing betatron oscillations. The entire translation from I to II occurs in less than half of a betatron oscillation. Because the drive laser overlaps the electron in (b) after it is trapped, the increased transverse momentum associated with DLA produces much larger amplitude betatron oscillations as shown at the point marked "III." (c) Trajectory of the test electron from (b) in the lab frame showing two complete betatron oscillations (black curve). These oscillations occurred when the electron was in the section marked III in Fig. 1(b). The green curve shows the transverse electric field sampled by the electron. The blue curve shows the DLA contribution to the final electron energy normalized to the maximum DLA contribution of 94 MeV. The unshaded and shaded regions indicate where the electron gains and losses, respectively, energy from DLA. Simulation parameters were: $a_0 = 2.1$, $w_0 = 6.7$ μm, $n_e = 8 \times 10^{18}$ cm^{-3} from a 99.9% He/ 0.1% N_2 neutral mix, and $\tau_{\text{laser}} =$ (a) 25 and (b) 45 fs.

and so we call this quantity the "DLA contribution" to the electron energy. The electrons that are executing betatron oscillations in the plane of the laser polarization will gain energy as long as the dot product $\mathbf{E}_\perp \cdot \mathbf{v}_\perp$ is a negative quantity (i.e., $\mathbf{E}_\perp$ is positive while $\mathbf{v}_\perp$ is negative or vice versa). Figure 1(c) shows the trajectory (black curve) of the sample electron shown in Fig. 1(b) while it executes two complete betatron oscillations as well as the $\mathbf{E}_\perp$ (green curve) that it samples along its trajectory. The electron has a negative $\mathbf{v}_\perp$ when its trajectory has a negative slope and a

positive $\mathbf{v}_\perp$ when it has a positive slope. The shaded regions mark where the electron loses energy to the transverse electric field because the dot product $\mathbf{E}_\perp \cdot \mathbf{v}_\perp$ is a positive quantity. In the unshaded regions, $\mathbf{E}_\perp \cdot \mathbf{v}_\perp$ is negative, and therefore the electron gains energy from the transverse electric field. The DLA contribution to the final energy of this electron was calculated using Eq. (1) and is shown (normalized to its maximum value) by the blue curve on Fig. 1(c). As expected, the DLA contribution increases in the unshaded regions, and that gain is largest when the electron crosses the laser axis and has the largest $\mathbf{v}_\perp$. This curve shows that although the energy exchanged between the electron and the transverse laser field oscillates, the electron gains net energy from DLA as expected since the electron is in an accelerating phase of $\mathbf{E}_\perp$ for more than one-half of each betatron oscillation.

In free space, the closest analog of the DLA process considered here is the inverse free electron laser mechanism [26–28] and the inverse ion channel laser [29]. The other so-called direct laser acceleration mechanism is acceleration in a dielectric [30] or plasma periodic [31,32] structure where the electric field of the laser pulse interacts with an electron in a periodic, slow-wave structure.

The experiments presented in this Letter used a 815-nm Ti:sapphire laser with a fixed pulse length τ_{laser} of 45 ± 5 fs full width at half maximum (FWHM) of intensity and a spot size w_0 of 6.7 μm. Laser powers P up to 5.6 TW were used, which gives a maximum vacuum intensity I_0 of 7.9×10^{18} W/cm^2 at focus, which corresponds to a normalized vector potential $a_0 \simeq 8.6 \times 10^{-10} \sqrt{I_0[\text{W/cm}^2]} \lambda[\mu m]$ of 2.0. An $F/6$ off-axis parabola focused the main laser pulse at the entrance of a variable-length (0.2–2 mm) gas cell [33,34]. The entrance and exit holes of the gas cell were drilled *in situ* by puncturing the front and rear walls using the laser pulse at a lower intensity. The diameters of the pinholes were between 150 and 300 μm. The plasma density n_e was measured on every shot using a Michelson interferometer and was varied by changing the gas pressure [33,34]. The electron beam was dispersed in energy with a 0.92 T dipole magnet onto a plastic scintillator or a lanex screen and recorded using a PI-MAX intensified CCD camera. A 6 μm (minimum thickness) aluminum filter shielded the scintillator or lanex from laser light. This entire electron spectrometer could be rotated by 90° so that the electrons could be dispersed either parallel or perpendicular to the laser polarization.

The extent to which the DLA mechanism contributes to the total energy gain of the electrons in such a nonlinear LWFA is dependent on the ratio of the laser pulse length relative to the nonlinear wake wavelength. This ratio will be represented by the dimensionless pulse length parameter

$$T_p = \frac{c\tau_{\text{laser}}}{\Lambda_{\text{wake}}} = \frac{\omega_p \tau_{\text{laser}}}{2\pi a_0^{1/2}}. \qquad (2)$$

If the laser pulse length $c\tau_{\text{laser}}$ is equal to the a_0-dependent length of the first bucket $\Lambda_{\text{wake}} \simeq \sqrt{a_0}[2\pi/(k_p)]$ [23], as is the case in Fig. 1(b), then $T_p = 1$. Here, $k_p = (\omega_p/c)$ and $\omega_p = \sqrt{[(e^2 n_e)/m\epsilon_0]}$ is the plasma frequency. Therefore, $T_p \sim 1$ indicates a significant overlap between the transverse laser field and the trapped electrons. In these experiments, $T_p \sim 1$, and with $a_0 \sim 2$ and $P \sim 2$–$3 ~ P_{\text{crit}}$, the LWFA was operating in the near-complete blowout [23] and self-guided regime [35]. In this case, electron self-trapping does not occur until the laser pulse undergoes considerable longitudinal and transverse compression [36,37]. In order to inject charge as early as possible in the interaction in a location where it overlaps the laser pulse, we used the ionization injection technique [14]. In this experiment, the gas cells were filled with 95% He and 5% N_2 gas using a pulsed solenoid valve.

Figure 2 shows two examples of the experimental electron spectra when the electrons were dispersed in the (a) same and the (b) orthogonal plane of the laser polarization for similar experimental parameters. When dispersed in the direction of the laser polarization, the measured electron beams exhibited a narrow divergence typical of LWFA. An example is shown in Fig. 2(a), where the electron beam has an average measured half width at half maximum (HWHM) divergence of 4.3 mrad for electron energies > 40 MeV. The continuous energy spread is characteristic of ionization injection [14,38]. However, when the electron beams were dispersed perpendicular to the laser polarization, they had a much larger divergence and additionally split at the highest electron energies, resulting in a forked structure. This behavior of the dispersed electron beam is shown in Fig. 2(b), where the average divergence increased to 11.8 mrad and the forked structure is clearly visible above 90 MeV. The divergence was calculated using the HWHM for electron energies below 90 MeV and using the fork
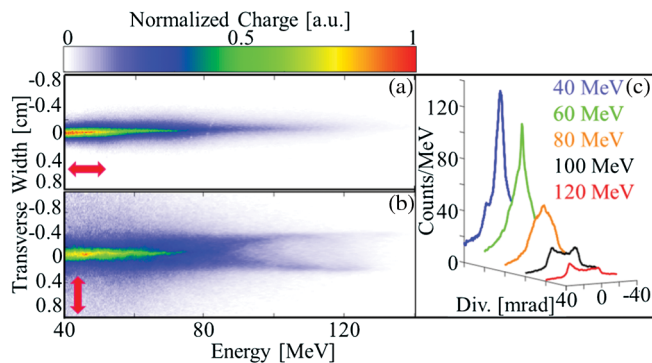

FIG. 2. (a),(b) Experimental electron spectra dispersed parallel and perpendicular, respectively, to the laser polarization (red arrows). The experimental parameters for the shots shown in (a) and (b) are gas cell length = 800 and 900 μm, $n_e = 1.7 \times 10^{19}$ and 1.4×10^{19} cm^{-3}, $a_0 = 2.0$ and 1.9, and $T_p = 1.1$ and 1.1, respectively. (c) Transverse lineouts of (b) at 20 MeV intervals.

centroid for energies above 90 MeV, which is where the fork structure begins. Such a fork structure has been consistently observed in experimental electron spectra for plasma densities between 0.9–1.5×10^{19} cm^{-3} ($T_p = 0.8$–1.3) [39]. In one set of data, 8 of 11 shots showed the emergence of a fork structure at the higher energies with the fork becoming more prominent for higher T_p values while the other 3 shots did not show a definitive fork structure [39]. The forked structure was never observed when the electron beam was dispersed parallel to the laser polarization. The undispersed electron beams in the range of densities explored here were elliptical with the major axis of the ellipse in the direction of the polarization of the laser beam. The transverse shape [Fig. 2(c)] of the spectrum clearly transitions from a center-peaked distribution to the forked structure. In the center-peaked distribution, the electrons gain the majority of their energy from LWFA and can originate from the first and subsequent buckets, in which the laser does not overlap the electrons. The electrons in the forked region of the spectrum originate in the first bucket of the wake and gain a majority of their energy via DLA, as we will show next.

We have carried out three-dimensional PIC simulations to interpret these observed features. These simulations modeled the above experimental parameters and employed particle tracking to elucidate the roles of LWFA and DLA to the energy gain of the electrons in this experimental regime. We used the code OSIRIS 3.0[40] with a moving window and the Ammosov-Delone-Krainov [41] ionization package. The grid was $1814 \times 320 \times 320$ with $2 \times 2 \times 2$ particles per cell and $k_0 \Delta z = 0.209$ and $k_p \Delta x, \Delta y = 0.120$. The resulting normalized time step was 0.01877. The laser in this simulation was linearly polarized with a central wavelength of 815 nm, a pulse length of 45 fs FWHM, and a focused spot size of 6.7 μm. The laser was focused to an a_0 of 2.03 halfway up a 100-μm density up ramp and then propagated through a 430-μm constant-density region before exiting through a 150-μm density down ramp. The laser ionized an initially-neutral gas comprised of 99.9% He and 0.1% N_2 to produce a plasma density of 1.43×10^{19} cm^{-3}. The laser self-focused [42] to a peak a_0 value of 4.0 at a distance of 20 μm into the constant-density region of the plasma. Its a_0 value then fell approximately linearly to a value of 2.9 at the exit of the constant-density region of the plasma. Despite this evolution, the self-trapping of He electrons in the simulation was negligible compared to the trapping due to ionization injection.

The simulation was run to completion once, and 550 electrons that were accelerating in the first bucket of the wake 30 μm before the start of the plasma down ramp were selected. The simulation was subsequently rerun to record the position, momentum, and fields sampled by each tagged electron at each time step of the simulation. To unravel the relative contributions of DLA and LWFA to the total energy gain of the electrons, the energy gain of these
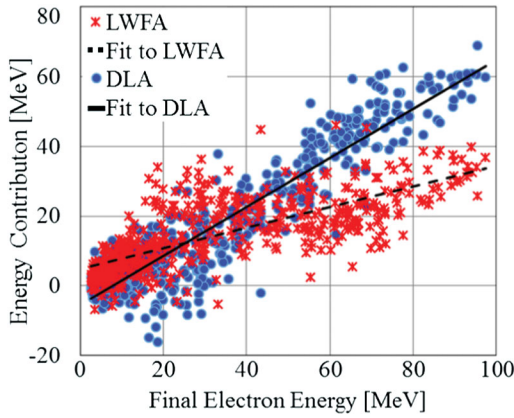
FIG. 3.   Plot of the DLA contribution $W_\perp$ (blue circles) and the LWFA contribution $W_\parallel$ (red stars) to the final energy of each of the 550 random electrons versus their final energies. The solid curve shows the best linear fit $E_{DLA} = 0.70 \, E_{final}$—5.36 [MeV] with an R^2 fit of 0.88 for the DLA contribution, and the dashed curve shows the best linear fit $E_{LWFA} = 0.30 \, E_{final} + 4.77$ [MeV] with an R^2 fit of 0.57 for the LWFA contribution.

tracked electrons due to the longitudinal electric fields $\mathbf{E}_\parallel$ was calculated using

$$W_\parallel = -e \int_0^t \mathbf{E}_\parallel \cdot \mathbf{v}_\parallel dt' \qquad (3)$$

at each simulation time step. Here, $\mathbf{v}_\parallel$ is the longitudinal velocity of the electron. The dominant longitudinal electric field is the wakefield, and so we will call the contribution calculated using Eq. (3) the "LWFA contribution." The LWFA and DLA contributions are plotted as a function of the final electron energy in Fig. 3. The best linear fits through those contributions show that the curves intersect at 25 MeV. Below this energy, the final electron energy is primarily dominated by LWFA, and above it, DLA becomes the dominant contribution.

As Fig. 3 shows, at final electron energies greater than 90 MeV, where we observed the forked structure in the experimental spectrum [Fig. 2(b)], the electrons have gained almost 2/3 of their energy from DLA. Because the energy gain from DLA relies on the coupling between the transverse laser field and the betatron motion of the electrons, a signature of this transverse coupling should be present in the energy gain of the electrons in the simulations as well. Indeed, as shown in Fig. 4(a), when the electron beam from the simulation is dispersed perpendicular to the laser polarization, it shows a forked structure similar to the experimental case in Fig. 2(b). Such a fork has been observed in simulations with T_p values between 0.8 and 1.4 but is not present in simulations (omitted for simplicity) where the laser pulse does not overlap the trapped electrons [$T_p \leq 0.5$, i.e., the case shown in Fig. 1(a)]. In Fig. 4(b), the randomly tagged electrons with energies 40 MeV and above are superimposed on a contour plot of the data
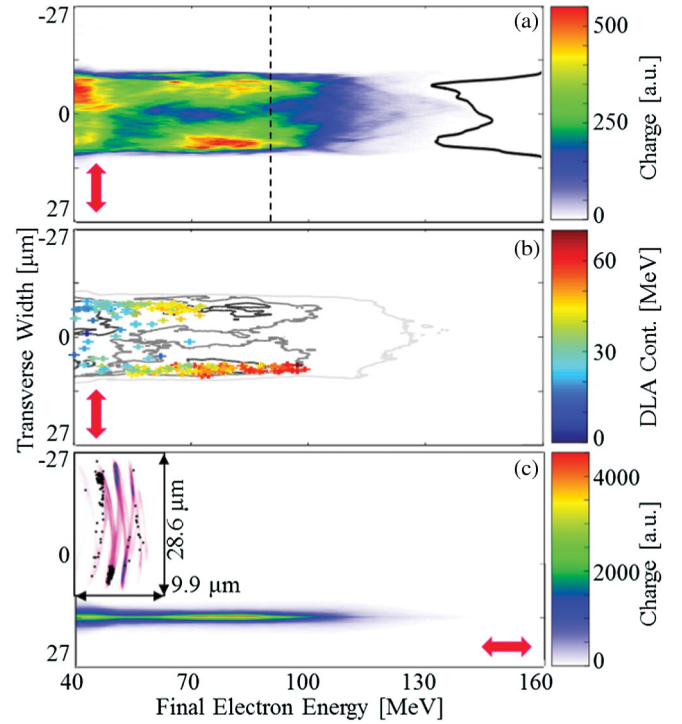

FIG. 4.   (a) Simulated electron spectrum perpendicular to the linear laser polarization (red arrows). The black curve shows the lineout of the forked structure at 90 MeV, which is marked by the black dashed line. (b) Contour plot of (a) showing the 4% (light gray line), 35% (dark gray line), and 61% (black line) contours. Crosses represent the randomly tagged electrons with energies over 40 MeV and are color coded by their DLA contribution. (c) Simulated electron spectrum parallel to the linear laser polarization. (Inset) Transverse profile of electron beam showing the electrons were primarily bunched at the extrema of their betatron oscillations when exiting the plasma. Black dots mark the randomly tagged electrons with energies over 40 MeV.

shown in Fig. 4(a). These electrons are color coded by their DLA contribution to the final energies. Those electrons that fall within the fork structure have the highest DLA contributions, and thus the fork shows a clear signature of DLA that was also seen in the experimental results of Fig. 2(b). The origin of the forked structure becomes evident when the transverse structure of the electron beam is examined. When DLA is present in a LWFA, the higher-energy electrons owe a significant portion of their energy to DLA. Consequently, as seen in the inset of Fig. 4(c), they tend to bunch at the extrema of their large-radii betatron oscillations [8] and therefore will exit the plasma with a transverse separation, which leads to a forked structure. Additional 3D simulations [39] (not shown) show that the center-peaked transverse shape of the experimental data shown in Figs. 2(b) and 2(c) is a signature of LWFA being the dominant energy mechanism for the lower-energy electrons. For further comparison with the experimental data, in Fig. 4(c), the simulated electron beam was dispersed in the direction of the laser polarization.

Similar to the experimental case shown in Fig. 2(a), the electron beam has a continuous energy spread and a narrow divergence; i.e., any structure associated with the enhanced oscillation of the electrons in the direction of the laser polarization cannot be discerned.

In conclusion, we have demonstrated experimentally and through supporting simulations that when there is a significant overlap between the trapped electrons and the laser in a LWFA cavity, the resulting electrons can gain comparable energy from both the LWFA and the DLA mechanisms. The DLA process in LWFA can be optimized further [9,10] and must be considered in LWFAs that employ other injection schemes [13].

---

[*]Present address: University of Rochester Laboratory for Laser Energetics.
jshaw05@ucla.edu
[†]Present address: Lawrence Livermore National Laboratory.
[‡]Present address: Stony Brook University.

[1] *Laser Acceleration of Particles*, edited by P. J. Channel, AIP Conference Proceedings, No. 91 (American Institute of Physics, New York, 1982).

[2] C. Joshi, Sci. Am. **294**, 40 (2006).

[3] T. Tajima and J. M. Dawson, Phys. Rev. Lett. **43**, 267 (1979).

[4] A. Pukhov, Z.-M. Sheng, and J. Meyer-ter Vehn, Phys. Plasmas **6**, 2847 (1999).

[5] A. Pukhov, Rep. Prog. Phys. **66**, 47 (2002).

[6] J. L. Shaw, F. S. Tsung, N. Vafaei-Najafabadi, K. A. Marsh, N. Lemos, W. B. Mori, and C. Joshi, Plasma Phys. Controlled Fusion **56**, 084006 (2014).

[7] J. L. Shaw, N. Vafaei-Najafabadi, K. A. Marsh, N. Lemos, F. S. Tsung, W. Mori, and C. Josh, arXiv:1502.07664v1.

[8] J. L. Shaw, N. Lemos, K. A. Marsh, F. S. Tsung, W. B. Mori, and C. Joshi, Plasma Phys. Controlled Fusion **58**, 034008 (2016).

[9] X. Zhang, V. N. Khudik, and G. Shvets, Phys. Rev. Lett. **114**, 184801 (2015).

[10] X. Zhang, V. N. Khudik, A. Pukhov, and G. Shvets, Plasma Phys. Controlled Fusion **58**, 034011 (2016).

[11] N. Lemos, J. L. Shaw, K. A. Marsh, and C. Josh, arXiv:1502.07764v1.

[12] S. Cipiccia et al., Nat. Phys. **7**, 867 (2011).

[13] N. Lemos, J. L. Martins, F. S. Tsung, J. L. Shaw, K. A. Marsh, F. Albert, B. B. Pollock, and C. Joshi, Plasma Phys. Controlled Fusion **58**, 034018 (2016).

[14] A. Pak, K. A. Marsh, S. F. Martins, W. Lu, W. B. Mori, and C. Joshi, Phys. Rev. Lett. **104**, 025003 (2010).

[15] C. McGuffey et al., Phys. Rev. Lett. **104**, 025004 (2010).

[16] S. Kneip et al., Phys. Rev. Lett. **100**, 105006 (2008).

[17] S. Kneip et al., in *Proceedings of SPIE*, Vol. 7359, edited by D. A. Jaroszynski and A. Rousse (SPIE Proceedings, 2009), p. 73590T.

[18] S. P. D. Mangles et al., Phys. Rev. Lett. **94**, 245001 (2005).

[19] C. Gahn, G. D. Tsakiris, A. Pukhov, J. Meyer-ter Vehn, G. Pretzler, P. Thirolf, D. Habs, and K. J. Witte, Phys. Rev. Lett. **83**, 4772 (1999).

[20] V. Malka et al., Phys. Plasmas **8**, 2605 (2001).

[21] P. M. Nilson et al., New J. Phys. **12**, 045014 (2010).

[22] M. Adachi, E. Miura, S. Kato, K. Koyama, S. Masuda, T. Watanabe, H. Okamoto, A. Ogata, and M. Tanimoto, Jpn. J. Appl. Phys. **45**, 4214 (2006).

[23] W. Lu, M. Tzoufras, C. Joshi, F. S. Tsung, W. B. Mori, J. Vieira, R. A. Fonseca, and L. O. Silva, Phys. Rev. ST Accel. Beams **10**, 061301 (2007).

[24] S. Wang et al., Phys. Rev. Lett. **88**, 135004 (2002).

[25] A. Rousse, Phys. Rev. Lett. **93**, 135005 (2004).

[26] R. B. Palmer, J. Appl. Phys. **43**, 3014 (1972).

[27] E. D. Courant, C. Pellegrini, and W. Zakowicz, Phys. Rev. A **32**, 2813 (1985).

[28] P. Musumeci, S. Y. Tochitsky, S. Boucher, C. E. Clayton, A. Doyuran, R. J. England, C. Joshi, C. Pellegrini, J. E. Ralph, J. B. Rosenzweig, C. Sung, S. Tolmachev, G. Travish, A. A. Varfolomeev, T. Yarovoi, and R. B. Yoder, Phys. Rev. Lett. **94**, 154801 (2005).

[29] D. H. Whittum, A. M. Sessler, and J. M. Dawson, Phys. Rev. Lett. **64**, 2511 (1990).

[30] A. Peralta et al., Nature (London) **503**, 91 (2013).

[31] A. G. York, H. M. Milchberg, J. P. Palastro, and T. M. Antonsen, Phys. Rev. Lett. **100**, 195001 (2008).

[32] S. J. Yoon, J. P. Palastro, and H. M. Milchberg, Phys. Rev. Lett. **112**, 134803 (2014).

[33] J. L. Shaw, N. Vafaei-Najafabadi, K. A. Marsh, and C. Joshi, *Proceedings of the Advanced Accelerator Concepts Workshop*, Vol. 315 (American Institute of Physics, 2013), p. 315.

[34] J. L. Shaw, master's thesis, University of California Los Angeles, 2013.

[35] J. E. Ralph, K. A. Marsh, A. E. Pak, W. Lu, C. E. Clayton, F. Fang, W. B. Mori, and C. Joshi, Phys. Rev. Lett. **102**, 175003 (2009).

[36] F. S. Tsung, W. Lu, M. Tzoufras, W. B. Mori, C. Joshi, J. M. Vieira, L. O. Silva, and R. A. Fonseca, Phys. Plasmas **13**, 056708 (2006).

[37] D. H. Froula et al., Phys. Rev. Lett. **103**, 215006 (2009).

[38] C. E. Clayton et al., Phys. Rev. Lett. **105**, 105003 (2010).

[39] J. L. Shaw, Ph.D. thesis, University of California Los Angeles, 2016.

[40] R. A. Fonseca et al., Lecture Notes in Computer Science, Vol. 2331 (Springer, Berlin, 2002), p. 342.

[41] M. Ammosov, N. Delone, and V. Krainov, Sov. Phys. JETP **64**, 1191 (1986).

[42] G.-Z. Sun, E. Ott, Y. C. Lee, and P. Guzdar, Phys. Fluids **30**, 526 (1987).